# Virtual four sensor fast response aerodynamic probe (FRAP®)

*Axel* Pfau*, *Joel* Schlienger†, *Anestis I.* Kalfas‡, and *Reza S.* Abhari§

ETH, Swiss Federal Institute of Technology, Turbomachinery Laboratory, Zurich, Switzerland

**Abstract.** This paper introduces the new fast response aerodynamic probe (FRAP®), which was recently developed at the ETH Zurich. The probe provides time-resolved, three-dimensional flow measurements using the virtual four sensor technique. Two probes work in tandem, being comparable to a pair of pneumatic needle probes. The first probe, being yaw angle sensitive, is positioned in three circumferential positions. The second probe being pitch angle sensitive is brought into exactly the same position as the first probe. The resulting set of four measurements is phaselock-averaged to one specific rotor trigger position. Then the reduced data sets are combined to four calibration coefficients, which are then further processed to determine the unsteady flow vector. The results consist of yaw and pitch flow angles as well as the total and static pressure. The outer diameter of the cylindrical probe head was miniaturized to 0.84mm, hence probe blockage effects as well as dynamic lift effects are reduced. The shape of the probe head was optimized in view of the manufacturing process as well as aerodynamic considerations. The optimum geometry for pitch sensitivity was found to be a cylindrical surface with the axis perpendicular to the probe shaft. The internal design of the probes led to a sensor cavity eigen frequency of 44 kHz for the yaw sensitive and 34kHz for the pitch sensitive probe. The steady aerodynamic characteristics of the probe were measured using the free jet probe calibration facility of the laboratory. The full set of calibration surfaces is given. Data acquisition is done with a fully automated traversing system, which moves the probe within the test rig and samples the signal with a PC-based A/D-board. An error analysis implemented into the data reduction routines revealed acceptable accuracy for flow angles as well as pressures for many turbomachinery flows. Depending on the dynamic head of the application the yaw angle is accurate within ±0.35° and pitch angle within ±0.7°. Finally, a comparison of time averaged results to five hole probe measurements is discussed.

## Nomenclature

| | | |
|---|---|---|
| C | Non-dim. Circumferential position | [-] |
| d | probe head diameter | [mm] |
| D | free jet diameter | [mm] |
| f | frequency | [Hz] |
| K | calibration coefficient | [-] |
| p | pressure | [Pa] |
| R | Non-dim. Radial height | [-] |
| U | Voltage | [V] |
| v | velocity | [m/s] |
| φ | yaw angle | [°] |
| γ | pitch angle | [°] |
| $C_p$ | non-dimensional pressure coefficient $C_p = \frac{p - p_{static}}{p_{total} - p_{static}}$ | [−] |

Probe 1 yaw angle sensitive probe
Probe 2 pitch angle sensitive probe

## 1 Introduction

With the design and build of the new 2-stage axial research turbine LISA [5] a new field of application to the FRAP measurement technology arose. The flow under investigation, the labyrinth leakage interaction in open cavities, was expected to be highly 3-dimensional in addition to being highly unsteady. Small scales of the cavities and the flow features demanded for a low blockage probes. Both requirements could not be satisfied with the existing single sensor probes.

Therefore, the development of a new miniature probe with 3-d capability was an important precondition to fulfill the project s research goals.

Three independent review papers on the unsteady pressure and flow measurement technologies based on silicon piezo-resistive sensors have been published: Ainsworth et al. [1], Sieverding et al. [6] and Kupferschmied et al. [4]. These papers together give a broad conspectus of the current state of the art.

* *Axel* Pfau: Axel.Pfau@flowtec.endress.com
† *Joel* Schlienger: joel.schlienger@swissonline.ch
‡ *Anestis I.* Kalfas: akalfas@auth.gr
§ *Reza S.* Abhari: abhari@lec.mavt.ethz.ch

## 2 Concept, design and construction

### 2.1 Measurement concept

The measurement concept is based on the idea of emulating a true four sensor probe with two single sensor probes. Figure 1 explains the way both probes work together in tandem. Probe 1 is turned into three positions similar to a virtual three sensor probe. Position 1 is the center position which is close to the total pressure of the flow. Due to the cylindrical surface of the head p2 and p3 give yaw angle sensitivity. To derive the pitch angle a forth measurement is necessary. In a second set up, probe 2 is positioned into exactly the same radial and angular position as probe 1 in position 1. The pressure on the inclined surface p4 compared with the pressure in position 1 gives yaw angle sensitivity.

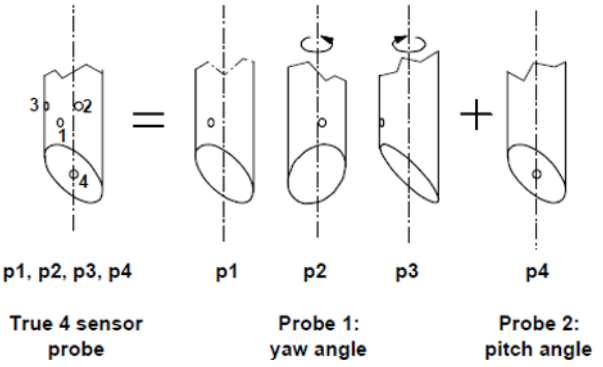


**Fig. 1.** Measurement concept of a virtual 4 sensor probe

All four pressure signals are brought together in a set of calibration coefficients representing a dimensionless yaw (Kϕ) and pitch angle (Kγ) and total (Kt) and static pressure (Ks) (see eq.1). The signals must be phase-lock-averaged to each other by an independent blade or rotor trigger signal. The stochastic portion of the unsteady signal is lost during the averaging procedure.

$$K_\varphi = \frac{p_2 - p_3}{p_1 - p_m}, K_\gamma = \frac{p_4 - p_5}{p_1 - p_m} \qquad (1)$$

$$K_t = \frac{p_{tot} - p_1}{p_1 - p_m}, K_s = \frac{p_1 - p_{stat}}{p_1 - p_m}$$

Where $p_m = \frac{1}{2}(p_2 + p_3)$

By using polynomial calibration models of the dependencies $\phi(K_\Phi,K_\gamma)$ and $\gamma(K_\varphi,K_\gamma)$ the flow angles can directly be derived out of the pressure signals. In a second step total and static pressure are calculated using polynomial calibration models of the form $K_t(\phi,\gamma)$ and $K_s(\phi,\gamma)$.

### 2.2 Probe head optimisation and design

To do the optimization of the head design a pneumatic probe with exchangeable head of 4mm head diameter was built and tested within the free jet calibration facility of the laboratory [3]. The head geometries were designed with view on the manufacturing process.
All probe head parts were wire eroded which only allows the creation of prismatic surfaces.

Out of this process an optimal design was deduced featuring a cylindrical surface whose center axis is perpendicular to the probe axis. The design is depicted in Figure 2. The diameter of the curvature was chosen to be 2.4 times the head diameter. The cylinder cuts the head such that it merges tangentially on the front side of the probe. The hole of the first probe, giving the yaw angle sensitivity, is placed at a distance of 1.1 mm to the tip. The second probe has a hole inclined under 45°, which gives pitch angle sensitivity. The hole to shaft diameter ratio is 0.3.

In Figure 3 the pitch sensitive calibration coefficient at 0° yaw angle is presented. At positive pitch angles around 25° the curve flattens and passes a maximum. The pitch angle sensitivity was found to be in average 50% higher than in the case of Gossweiler's [2] geometry.

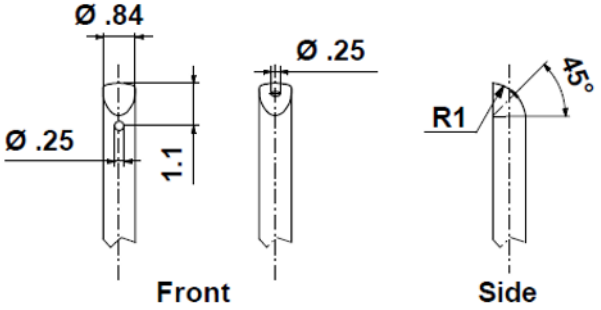


**Fig. 2.** Final probe head design

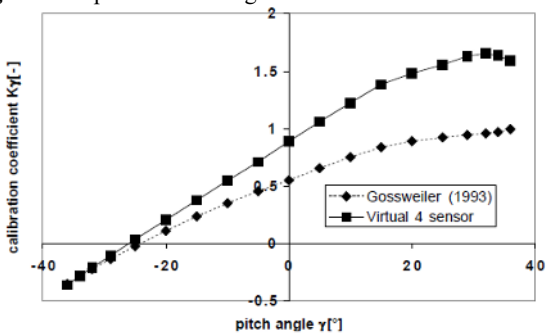


**Fig. 3.** Comparison of calibration coefficient: Gossweiler [2] and virtual 4 sensor probe, φ = 0°

### 2.3 Manufacturing

The manufacturing technology is based on consequent miniaturization of the probe head components and the sensor packaging, which surround the sensor. The sensor has the dimensions of 1.6x0.6x0.4mm. The probe head consists of three parts, which were wire. The wire has a diameter of 0.05mm, which defines the smallest possible structure. The base part integrates the reference pressure channel and the side walls, which align and protect the sensor. The sensor is glued into it using a soft silicon adhesive. Different thermal expansion coefficient of the base metal and the sensor material are compensated within the silicon layer such that thermal stresses are not induced into the sensor.

To complete the probe heads outer shape two parts, a long and a short cover, are glued onto the base part. The short cover is made in two different versions: one with a hole on the stem cylinder the other having no hole. The size of these parts are at 0.84x0.6x0.3mm. In order to

achieve pitch angle sensitivity a hole is introduced into the pitch angle sensitive surface.

A reference pressure tube and wires are connected to the probe head Both, tube and wires, lay within a shaft of 2.5mm, which connects to the main shaft of 6mm outer diameter. At the end of the shaft a small box containing the amplifier completes the probe.

Altogether, an estimated 40 different mechanical and micro-mechanical steps of several hours each are necessary to build one probe. Each step is followed by a hardening time of at least 6 hours. This sums up to 500 hours of elapsed time per probe. The finished pair of probes is presented in Figure 4.

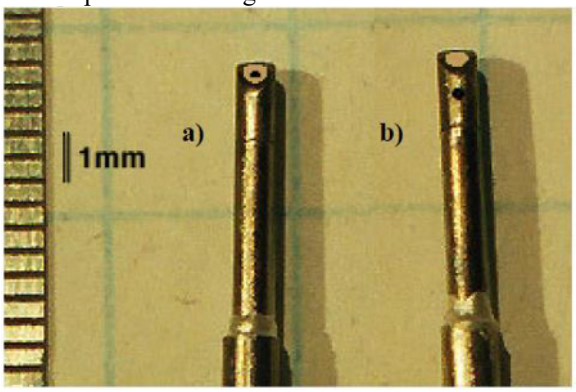


**Fig. 4.** a) pitch angle sensitive probe b) yaw angle sensitive probe

## 3 Probe sub system and calibration

### 3.1 Sensors

The pressure sensors working principal is the Wheatstone bridge. The bridge is fed by a constant current source of 1mA. The excitation voltage $U_e$ and the signal voltage U are amplified by the factor of 100 and measured. Thereby the excitation voltage is a measure for the membrane temperature and the signal voltage is proportional to the differential pressure across the membrane. The sensors, which were build into the probes, have a sensitivity of 8.1mV/mbar for probe 1 and 7.8 mV/mbar for probe 2 after amplification.

Each sensor needs to be calibrated individually. The calibration procedures described in Kupferschmied [3] were applied in this case. To derive a sensor calibration model the probe head is exposed to a constant temperature air stream of low velocity (5m/s) within a calibration oven. The temperature steps chosen for this calibration were 15, 25, 35, and 45ºC. Each temperature plateau was held for at least 4 hours to ensure temperature equilibrium. During each temperature step pressure cycles of 6 different levels are applied to the reference pressure tube. The pressure range covered by this calibration was 2 to 45 kPa. The amplified signal of the sensor is measured and stored, automatically.

The gathered data is used to get the relationship of voltages to pressure $p(U,U_e)$ and temperature $T(U,U_e)$. This is performed via a 2 dimensional polynomial interpolation of 2nd order in both directions.

It has been previously known that the type of sensors used here are affected by a time depending offset drift of the signal U while the excitation voltage $U_e$ stays relatively constant with time. The drift affects the offset of the sensor but not its sensitivity. To account for the effect of drift the offset of the sensor must be known during measurements with the probes. Therefore, an adjustment procedure is applied to the probes before and after each measurement task. While a measurement campaign is running the probes must be brought into an environment, where the pressure at the probe tip is known. This can be achieved by pulling the probe out of the flow regime into a settling chamber where the fluid is at a rest and the static pressure can be measured. Then two pressure levels are applied to the reference pressure tube and U and $U_e$ are measured. The resulting two adjustment coefficients affect the offset the gain of the sensor model, respectively.

An additional undesirable behavior of the piezo-resistive sensor is the effect of self heating. If the air around the probe head is at a complete rest the heat produced in the sensor is not convected away. This leads to a higher sensor membrane temperature and therefore also to a higher temperature reading of the probe ($U_e$). Investigating this effect it was found that a velocity step from 5m/s to 0m/s and back to 5m/s resulted in a temperature change in both step directions of 2ºC. This implies that good quantitative steady temperature measurements are difficult to achieve.

Concentrating on accurate pressure measurement, the sensor adjustment and evaluation procedures were optimised and tested against a first order accurate pressure measurement device. The accuracy of pressure evaluation was found to be ±20Pa for both probes covering the pressure range of application 0...30kPa, which equals to 0.07% FS. This result was also found to be true across velocity step of 5 to 0m/s and back where all velocity conditions were kept constant for one hour.

### 3.2 Steady aerodynamic

The steady aerodynamic behavior of the probe determines the calibration range in yaw and pitch angle. It is evaluated by measuring in a well defined steady flow environment. The free jet probe calibration facility is described by Kupferschmied (1998) allowing a yaw angle variation of ±180º and pitch angle variation of ±36º.

In Figure 5 the non-dimensional pressure readings $C_p$ of both probes for varying yaw angle at a constant pitch angle of 0º are depicted. The data are extracted from the aerodynamic calibration data, which in view of the application comprises of two Mach-numbers 0.15 and 0.3. For the yaw angle sensitive probe 1 the $C_p$ becomes 0 at a turning angle of ±45º. These positions were chosen to measure positions 2 and 3 in the measurement concept (see also Figure 1).

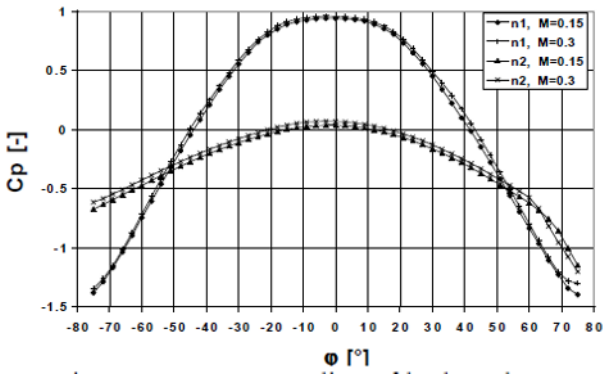


**Fig. 5.** Pressure reading of both probes at 0° pitch angle and two Mach-numbers, M = 0.15, 0.3

Changes in pressure distribution due to Mach number variations are small. The Reynolds-number based on the head diameter is $Re_d$=2400 at the lower and $Re_d$=4800 at the higher Mach-number. This is well within the subcritical range of $10^3$ to $10^5$ where the drag coefficient of the probe head stays constant. Therefore, any viscosity effects on the probe head can be omitted for a range above a Mach number of 0.06.

The set of calibration data was taken on an equidistantly spaced grid covering ±30° in yaw and pitch angle. The chosen mesh width of 3° resulting in 21x21 points. The data was non-dimensionalized to correct for the change in atmospheric pressure.

Since positions 2 and 3 are shifted by 45° and 45° respectively, the absolute range of probe yaw angle positions to calculate $C_{p2}$ and $C_{p3}$ are 15°....75° and -75°...-15°. In Figure 6 the pressure distribution of position 4 is shown. It can be seen that pitch angle sensitivity is decoupled from yaw angle position. Like in Figure 3 the nondimensional pressure flattens for pitch angles around 24°.

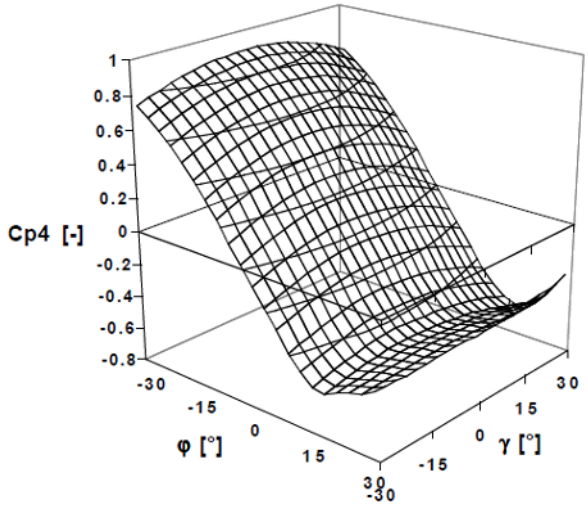


**Fig. 6.** Non-dimensional pressure $C_{p4}$, M = 0.3

With equation 1 all calibration coefficients are defined. According to the Cp definition, $Cp_{tot}$ and $Cp_{stat}$ have values of 1 and 0, respectively. To get the mathematical representation of the calibration the coefficients are interpolated by using 2 dimensional polynoms of 6th order for the flow angles and 4th order for total and static pressure coefficients. The polynomial coefficients are found by using the least square method. The resulting functions are $\varphi(K_\varphi,K_\gamma)$, $\gamma(K_\varphi,K_\gamma)$ and $K_t(\varphi,\gamma)$, $K_s(\varphi,\gamma)$.

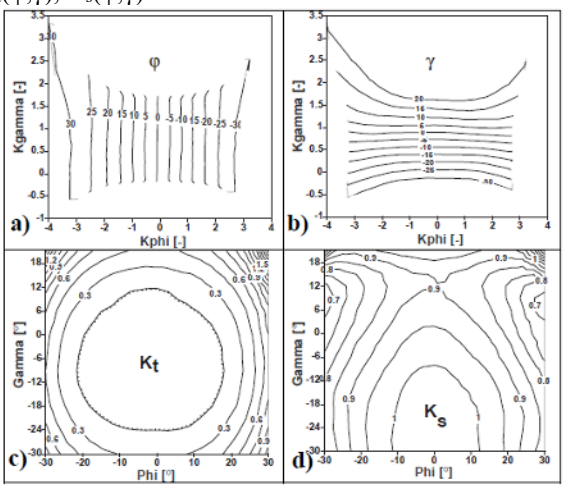


**Fig. 7.** Aerodynamic calibration surfaces: φ, γ, $K_t$, $K_s$

In order to get a working aerodynamic model, the calibration range had to be limited in positive pitch angle direction to 21°. For values higher than 21° the results of the angle evaluation would be ambiguous due to the flattening of the Cp4 distribution, see Figure 6. Therefore, the calibration limits can be given to ±30° in yaw and -30° to 21° in pitch angle. In Figure 7 the calibration surfaces are shown. The lines of constant ϕ and γ in Figure 7a and b are normal to each other, which shows the desired decoupling of both calibration coefficients $K_\phi$ and $K_\gamma$. Only in the corners of the calibration range orthogonality gets distorted. That is also the region where the highest residuals in the polynomial interpolation occur. The yaw and pitch angle sensitivity defined as $\frac{\partial K_\varphi}{\partial \varphi}$ and $\frac{\partial K_\gamma}{\partial \gamma}$ at ϕ=0° and γ=0° are 0.09 and 0.032, respectively. For $K_t$ values around 0 are expected. In the extremes of the calibration range $K_t$ becomes as high as 1.8. In most parts Ks shows values around 1.

### 3.3 Frequency response

Two different aerodynamic effects influence the frequency response of a FRAP probe. The pneumatic cavity between the pressure tab and the sensor membrane is one source of influence. Associated with the characteristic length of the cavity is an acoustical resonance. It causes higher amplitudes and shifted phase of the signal in a frequency range around the eigen frequency. The other stems from the fact that probes are intrusive to the flow, resulting in a distortion of the flow field at the location of measurement. The vonKarman vortex street downstream of a cylindrical body can also affect the measurements at the probe tip due to fluctuating flow vectors. In addition to these aerodynamic effect, mechanical vibrations of the probe shaft might also alter the frequency response of the probe. The mechanical eigen frequency of the sensor membrane is very high (around 500kHz Gossweiler [2]) and therefore plays no role in this type of application.

An estimate of the eigen frequency of both pneumatic cavities was obtained in the free jet. The turbulent total pressure fluctuations at the edge of the jet were sufficient

to acoustically excite the cavity in a broad spectrum of frequency. In order to have the same kind of excitation for both probes, both probes were positioned such that the holes were facing the flow. Then the data were Fourier analyzed. The result of these measurements is given in Figure 8.

In the right part of the diagram the eigen frequencies of both pneumatic cavities are present; 44 kHz for probe 1 and 34 kHz for probe 2. Both values are close to the eigen frequency of the miniature pitot described by Kupferschmied [3], which is 46 kHz. The larger cavity of probe 2 is due to the internal design, reflecting in the lower eigen frequency.

From the present application a correction of the pressure signal of the probes based on a transfer function is not considered necessary. The highest frequency expected in the test rig, 15 kHz, is well away from the first rise in amplitude at 30 kHz. For frequencies lower than 15 kHz no change in amplitude and phase is expected.

This diagram also gives the opportunity to discuss mechanical vibrations of the shaft due to aerodynamically induced forced response. On the left hand side three sharp peaks occur having frequencies of 0.7 kHz, 5.7 kHz and 9.7 kHz.

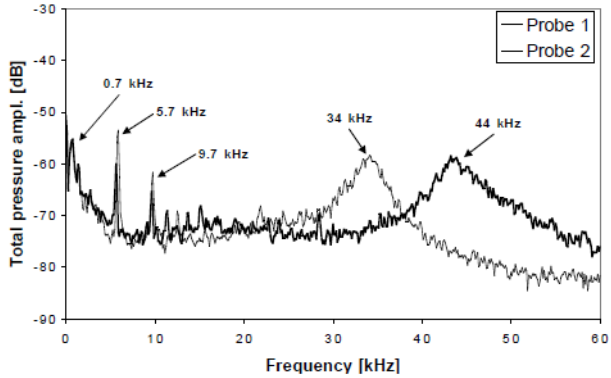


**Fig. 8.** FFT of the pressure signal within the free jet

The lower frequency can be calculated using the mode shape equation of a prismatic beam (equation 2).

$$f = \frac{\lambda^2}{2\pi l^2}\sqrt{\frac{EI}{\rho A}} \quad (2)$$

The first mode has a λ of 1.875. The shaft length from the point of clamping until the transition of the large stem to the next stem was l=85mm. The equation gives a first mode frequency of this part of the stem of 715 Hz, which is reasonable close to the measurement. Further experimental investigations on the origins of the mechanical vibrations are planned at a later time.

Using the probe within the turbine test rig those mechanical vibrations were not observed. The length of clamping there was 400mm, reducing the eigen frequencies substantially.

### 3.4 Error analysis

The error calculation was implemented directly into the evaluation program, whose structure follows Figure 9. It is based on the error propagation equation (3) with F=f(x,y,...) following the scheme of Treiber and Kupferschmied. [7].

$$\Delta F = \pm\sqrt{\left(\frac{\partial F}{\partial x}\Delta x\right)^2 + \left(\frac{\partial F}{\partial y}\Delta y\right)^2 + \cdots} \quad (3)$$

Starting point of the error calculation was the differential pressure measured with the sensors. The process of evaluating the sensor voltages, including the offset and gain correction coefficients J1 and J2, was found to be accurate to within ±20Pa against a first order accurate pressure measurement device.

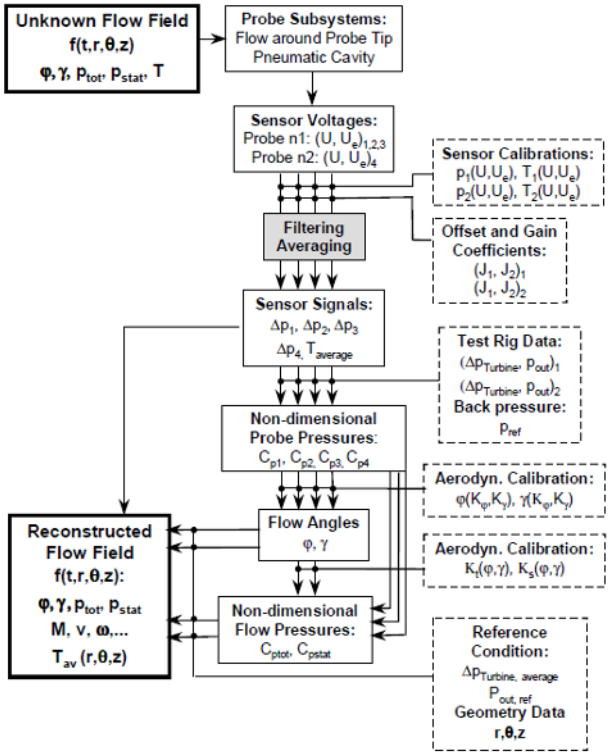


**Fig. 9.** Signal paths from flow to measurement results

A list of resulting uncertainties is given in Table1. Two characteristic cases, the flow downstream of a rotor (M=0.1) and the flow downstream of a stator (M=0.35) were investigated. A higher dynamic head is of course beneficial to the absolute accuracy of the flow angles, as the calibration coefficients are inversely proportional to the dynamic head. The total pressure is less accurate than the static pressure since the residuals of the polynomial model are higher and contribute to the error. One possibility to achieve a lower error would be to partition the calibration surface in additional areas. With that, the polynomial approximation would get closer to the points of calibration values.

Looking at the relative accuracy of the local dynamic head downstream of the stator the errors of total and static pressure add up to 3.5% of dynamic head. Downstream of the rotor this becomes 12% of dynamic head. At even lower Mach numbers the measurement accuracy becomes less. Experience shows that the lowest velocity at which the probe is still giving in that sense reasonable data is M=0.06.

**Table 1.** Typical error band width of flow parameters

| Parameters | Rotor Exit | Stator Exit |
|---|---|---|
| φ | ±1° | ±0.35° |
| γ | ±2° | ±0.7° |
| Cptot | ±0.0025 | ±0.0033 |
| Cpstat | ±0.0012 | ±0.0022 |
| ptot | ±80Pa | ±120Pa |
| pstat | ±60Pa | ±85Pa |

# 4 Proof of concept

## 4.1 First measurements and data reduction

The results presented in this chapter stem from a first measurement campaign within the new, two stage axial turbine LISA . The plane of measurement was positioned downstream of the second stator in mid axial position between stator trailing edge and rotor leading edge. The position is pointed out in Figure 10. The test rig was running at design operation point and the tip clearance was set to 0.3% of span.

The measurement plane was first measured with a pneumatic five hole probe. From these results the time-averaged flow angles were obtained. Then, the optimal turning angle of the virtual four sensor probe at each measurement position was derived, such that the angle fluctuation would happen around zero degrees.

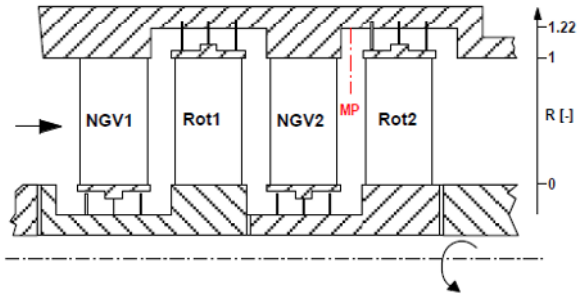


**Fig. 10.** Cross section of the test turbine with measurement position

The measurements utilize the yaw angle sensitive probe followed by the pitch sensitive probe. The rig was kept on operating to ensure same operation point conditions. Mechanical precision of mounting and traversing the probe is crucial to the measurement concept since both probes must be positioned into exactly the same locations. The mounting procedure for both probes is repeatable in the order of ±0.1mm in radial extent and ±0.05° in turning angle. 21 circumferential positions per blade pitch were measured where the accuracy of these positions (±0.05mm) was ensured by an encoder.

The measurement task files run as radial immersions into the flow field taking three turning angle positions (0°, ±45°) at each radial position for the yaw angle sensitive probe and the 0° angular position for probe 2. The measurement locations range from cavity bottom over the secondary loss core of the stator tip end wall flow which is located at 75% span. In general 16 measurement position were applied in radial direction. This results in 368 measurement points per plane. Before and after each radial traverse the offset and the gain of the sensor was measured by applying two pressure levels to the reference pressure tube. Each measurement position is sampled 3 seconds at a rate of 200kHz which results in 13 Gbytes of raw data per measurement plane.

In a first step of the data processing 100 data sets phase, locked to one specific trigger position on the rotor circumference, are cut out of the raw data and saved in a file. Each data set covers three consecutive passages at 106 samples per passage. To this raw the calibration model with the sensor adjustment coefficients is applied, providing the differential pressure and absolute temperature of the sensor. The pressure data is filtered using a zero-phase digital filtering algorithm, see Figure 9. The filter characteristic is a 7th order Butterworth filter of 15 kHz cut off frequency. The filtered pressure signals then are phase lock averaged using 100 samples at each instant of sampling. The phase lock averaged pressures are non-dimensionalised by using the static pressure at the exit of the turbine and the total pressure at the turbine inlet and then passed through the aerodynamic model. With geometric information about the probe tip position the results can be transformed into the test rig coordinate system. Now all further flow quantities, like absolute or relative Mach-number, and velocity components can be calculated.

## 4.2 Comparison to five hole probe data

In Figure 11 the non-dimensional, time averaged total pressure measured with the virtual four sensor probe and the pneumatic five hole probe data are brought together. The direction of view is upstream onto the trailing edge of the stator. The dashed line depicts the tip radius of the main flow annulus. The cavity bottom has a radial height of 1.22 (see also Figure 11 top). Figure 11c shows the difference between both measurement technologies.

Both probes capture the basic steady flow phenomena including the loss core at 75% radial height. It is connected to the wake at lower radii. Secondly, the strong total pressure gradient, which connects the cavity flow to the main flow, is found in both cases at a radial height of 95%. It is of the order of 900Pa/mm. The shapes of the total pressure contours are virtually the same: On the pressure side of the wake the high gradient flow reaches the tip radius. On the suction side, it enters the main flow duct as far as 92% radial height. A sudden change in the direction of the gradient is bridging the suction side feature with the pressure side feature at C=-0.1 and R=0.97.

The difference of both results, as it is visualized in Figure 11c, show a good agreement of level (±0.002) in the main flow out side the loss core as well as in 50% of the cavity flow area. This is well within the uncertainty band given in Table 1. Areas of higher differences are found in the region of high total pressure gradient, at the upper right and lower left part of the loss core and within the cavity.

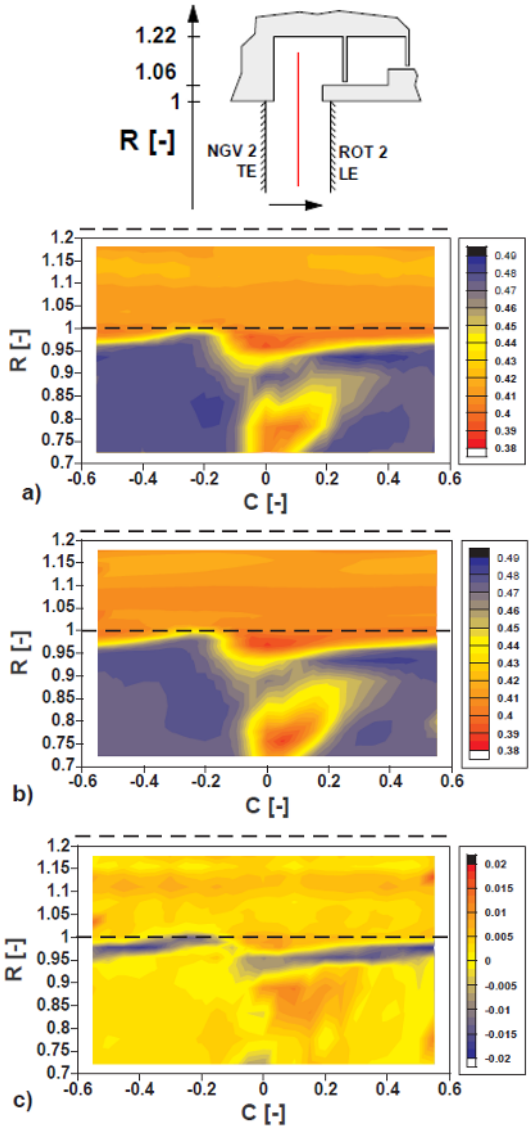


**Fig. 11.** Comparison of non dimensional total pressure $C_p$: a) virtual 4 sensor probe, b) 5 hole probe, c) difference a-b

In strong radial total pressure gradients the virtual four sensor probe measures up to 600Pa lower total pressure than the five hole probe. The blue ribbon is disconnected at the location where the radial total pressure gradient turns over into a circumferential total pressure gradient (C=-0.1, R=0.97). Total pressure gradients may affect both types of probes. A sensitivity study on the aerodynamic model of the five hole probe revealed that the total pressure gradients of this magnitude may result in a pitch angle error of around 0.5°. But yaw angle as well as total and static pressure stay unaffected. Therefore, it is important to look at the radial positioning of the probes again. A difference in probe tip location of 0.3mm in radial position in this region may result in a total pressure difference of 270Pa.

## 5 Conclusions

A novel miniature fast response aerodynamic probe (FRAP) has been developed, built and tested. It is based on the measurement concept of a virtual four sensor probe. It can measure three dimensional and unsteady flow up to frequencies of 25kHz covering flow angles of ±30° in yaw and -30° to +21° in pitch direction.

The unique miniature size of the probe of 0.84 mm diameter is a necessity for the use of the probe in labyrinth cavities. It is also at the mechanical limit of miniaturization which can be achieved with the current sensor.

With this probe a new useful measurement technique is at hand to study the 3D unsteady flow field.

## 6 Acknowledgments

We would like to extend our thanks to P. Kupferschmied who shared his knowledge on probe manufacturing. Without an excellent technical support, in particular T. K nzle, this probe would not have been possible.

The flow measurements in the turbine were supported by the German Federal Ministry of Economy (BMWI) under file numbers 0327060D and 0327060F. The authors gratefully acknowledge AG Turbo, Alstom Power and Rolls-Royce Germany for their support and permission to publish figures of the flow field in this paper.

## References

1. R. S. Ainsworth, R. J. Miller, R. W. Moss, S. J. Thorpe, *Unsteady pressure measurement*, Meas. Sci. Technol., **11**, p1055-1076 (2000)
2. C. Gossweiler, *Sonden und Messsystem f.r schnelle aerodynamische Str.mungsmessung mit piezoresistiven Druckgebern*, ETH dissertation **10253**, Zürich, Switzerland (1993)
3. P. Kupferschmied, *Zur Methodik zeitaufgel.ster Messungen mit Str.mungssonden in Verdichtern und Turbinen*, ETH dissertation **12774**, Zürich, Switzerland (1998)
4. P. Kupferschmied, P. Koppel, W. Gizzi, C. Roduner, G. Gyarmathy, *Time-resolved flow measurements with fast-response aerodynamic probes in turbomachines*, Meas. Sci. Technol., **11**, p1036-1054 (2000)
5. M. Sell, J. Schlienger, A. Pfau, M. Treiber, R. S. Abhari, *The 2-stage axial turbine test facility LISA*, Proceedings of the ASME Turbo Expo, 2001-GT-492, June 4-7, New Orleans, Louisiana (2001)
6. Ch. Sieverding, T. Arts, R. Denos, J. F. Brouckaert, *Measurement Techniques for unsteady flows in turbomachines*, Exp. Fluids, **28**, No.4, pp 285-321 (2000)
7. M. Treiber, P. Kupferschmied, *Analysis of the error propagation arising from measurements with a miniature pneumatic 5-hole probe*, Proceedings of the 13th symposium on measuring techniques for transsonic and supersonic flows in cascades and turbomachines, Limerick,Ireland (1998)